Remote Sensing of Environment 210 (2018) 65–75

Contents lists available at ScienceDirect

Remote Sensing of Environment

journal homepage: www.elsevier.com/locate/rse

How far are we from the use of satellite rainfall products in landslide forecasting?

M.T. Brunetti[a,*], M. Melillo[a], S. Peruccacci[a], L. Ciabatta[a,b], L. Brocca[a]

[a] CNR IRPI, via Madonna Alta 126, 06128 Perugia, Italy
[b] Department of Civil and Environmental Engineering, University of Perugia, Italy

ARTICLE INFO

Keywords:
Remote sensing
Landslide
Rainfall threshold
Italy
Soil moisture

ABSTRACT

Satellite rainfall products have been available for many years (since '90) with an increasing spatial/temporal resolution and accuracy. Their global scale coverage and near real-time products perfectly fit the need of an early warning landslide system. Notwithstanding these characteristics, the number of studies employing satellite rainfall estimates for predicting landslide events is quite limited.

In this study, we propose a procedure that allows us to evaluate the capability of different rainfall products to forecast the spatial-temporal occurrence of rainfall-induced landslides using rainfall thresholds. Specifically, the assessment is carried out in terms of skill scores, and receiver operating characteristic (ROC) analysis. The procedure is applied to ground observations and four different satellite rainfall estimates: 1) the Tropical Rainfall Measurement Mission Multi-satellite Precipitation Analysis, TMPA, real time product (3B42-RT), 2) the SM2RASC product obtained from the application of SM2RAIN algorithm to the Advanced SCATterometer (ASCAT) derived satellite soil moisture (SM) data, 3) the Precipitation Estimation from Remotely Sensed Information using Artificial Neural Network (PERSIANN), and 4) the Climate Prediction Center (CPC) Morphing Technique (CMORPH). As case study, we consider the Italian territory for which a catalogue listing 1414 rainfall-induced landslides in the period 2008–2014 is available.

Results show that satellite products underestimate rainfall with respect to ground observations. However, by adjusting the rainfall thresholds, satellite products are able to identify landslide occurrence, even though with less accuracy than ground-based rainfall observations. Among the four satellite rainfall products, CMORPH and SM2RASC are performing the best, even though differences are small. This result is to be attributed to the high spatial/temporal resolution of CMORPH, and the good accuracy of SM2RSC. Overall, we believe that satellite rainfall estimates might be an important additional data source for developing continental or global landslide warning systems.

1. Introduction

Worldwide, rainfall-induced landslides occur every year causing fatalities, considerable damage and relevant economic losses. Italy is one of the countries most prone to landslide risk (Guzzetti et al., 2005) and where the population is heavily affected. In the 50-year period 1964–2013, 1354 people died due to landslides (Salvati et al., 2014). Moreover, climate changing is expected to exacerbate the impact of landslides, mostly due to the increase in heavy rainfall (Fischer and Knutti, 2015; Ciabatta et al., 2016; Gariano and Guzzetti, 2016). In order to mitigate landslide risk, early warning systems for the prediction of rainfall-induced failures were developed in several countries based on different approaches and input data sets (Keefer et al., 1987; Baum and Godt, 2010; Rossi et al., 2012; Lagomarsino et al., 2013; Segoni et al., 2015; Piciullo et al., 2016). The forecast of rainfall-induced landslides relies upon physically-based (e.g., Baum et al., 2010; Lepore et al., 2013; Segoni et al., 2010; Alvioli and Baum, 2016) or empirical rainfall thresholds (e.g., Caine, 1980; Innes, 1983; Aleotti, 2004; Guzzetti et al., 2007; Guzzetti et al., 2008; Brunetti et al., 2010; Peruccacci et al., 2012). Empirical rainfall thresholds are calculated analyzing past rainfall events that have or have not resulted in landslides. In operational landslide warning systems, empirical rainfall thresholds are compared with rainfall measures, estimates, and forecasts to evaluate the possible occurrence of failures. Guzzetti et al. (2007) grouped empirical rainfall thresholds in three main categories: (i) thresholds using rainfall measures for a specific rainfall event (e.g., mean rainfall intensity-rainfall duration *ID* thresholds, Aleotti, 2004; Brunetti et al., 2010; Berti et al., 2012; Martelloni et al., 2012; Rosi

* Corresponding author.
E-mail address: mariateresa.brunetti@irpi.cnr.it (M.T. Brunetti).

https://doi.org/10.1016/j.rse.2018.03.016
Received 23 June 2017; Received in revised form 9 March 2018; Accepted 11 March 2018
Available online 17 March 2018

et al., 2012); (ii) thresholds considering the antecedent conditions (e.g., explicitly including rainfall and/or SM, Crozier, 1999; Glade et al., 2000; Ponziani et al., 2011; Brocca et al., 2012; Chen et al., 2017); and (iii) other thresholds. To date, the *ID* and the cumulated rainfall-rainfall duration *ED* thresholds (e.g., Peruccacci et al., 2012; Vennari et al., 2014; Gariano et al., 2015; Giannecchini et al., 2016) are the most used worldwide.

The accurate estimation of rainfall is the primary task in all the early warning systems mentioned above, and the reliability of the final forecasts is strongly dependent on the quality of rainfall inputs (Hong et al., 2006). Specifically, the spatial-temporal occurrence and the number of landslides are dependent on different rainfall attributes such as rainfall climatology, antecedent rainfall accumulation, rainfall intensity, cumulated event rainfall and duration. In the scientific literature, the vast majority of studies developing landslide forecasting systems used rain gauge measurements (e.g., Baum and Godt, 2010). However, it is well known that rain gauge observations are affected by several errors, primarily related to their small spatial representativeness, but also to the measurement accuracy (Nikolopoulos et al., 2014; Marra et al., 2017a). Additionally, the maintenance of real-time rain gauge networks is costly and not easy to achieve, mainly when networks operate in extreme weather conditions. The use of rain gauges for rainfall monitoring is less applicable in many parts of the world in which rain gauge networks have very low density, or even they are absent (Kidd et al., 2017). To overcome this issue, in the last three decades remote sensing observations have been used for providing rainfall estimates on a global scale at ever increasing spatial/temporal resolution and accuracy. The Satellite Application Facility on Support to Operational Hydrology and Water Management (H SAF, http://hsaf.meteoam.it/, Mugnai et al., 2013), the Tropical Rainfall Measurement Mission (TRMM) Multi-satellite Precipitation Analysis (TMPA, Huffman et al., 2007), and the recent Global Precipitation Measurement (GPM, https://pmm.nasa.gov/GPM, Hou et al., 2014) mission are examples of project and missions addressed to the development of satellite-based rainfall products. The first attempt of using satellite rainfall product by TMPA for global landslide hazard assessment was carried out by Hong et al. (2006, 2007) who performed a preliminary analysis for assessing the capability of a global system in predicting the occurrence of large landslide events worldwide. The system was further updated and improved by Kirschbaum et al. (2009, 2012), who highlighted some issues in the original system due to the spatial resolution of the susceptibility map and the need to re-compute the *ID* threshold for better considering regional climatology. The system was made operational at https://trmm.gsfc.nasa.gov/publications_dir/potential_landslide.html and it will be updated by replacing TMPA product with the new GPM data, with expected improved performances (Sidder, 2016). Another study was carried out by Farahmand and AghaKouchak (2013) who implemented a satellite-based global landslide model but using a different precipitation product, i.e., the Precipitation Estimation from Remotely Sensed Information Using Artificial Neural Networks, PERSIANN (Hsu et al., 1997; Sorooshian et al., 2000) and a machine learning approach as landslide prediction model. More recently, some authors employed satellite precipitation data for regional and local scale analyses (Liao et al., 2010; Kirschbaum et al., 2015; Robbins, 2016; Cullen et al., 2016; Rossi et al., 2017; Marra et al., 2017b; Nikolopoulos et al., 2017). Specifically, Marra et al. (2017a) investigated the effect of spatial aggregation due to satellite rainfall product in the assessment of rainfall threshold for debris flow occurrence prediction. Nikolopoulos et al. (2017) evaluated different satellite rainfall products for debris flow prediction over the upper Adige River basin in the eastern Italian Alps. A couple of studies employed both soil moisture (SM) estimates and satellite-based precipitation in order to monitor independently initial conditions and rainfall and, hence, better forecast landslide occurrence (Ray and Jacobs, 2007; Posner and Georgakakos, 2015; Cullen et al., 2016). Ray and Jacobs (2007) used the Advanced Microwave Scanning Radiometer (AMSR) for monitoring antecedent SM conditions and TMPA for estimating precipitation at three sites worldwide (California, Nepal and Philippines). A clear relationship between landslide occurrence and high SM and precipitation conditions as estimated by satellite sensors was highlighted.

Based on the brief literature review reported above, it is evident that satellite-based rainfall estimates have been scarcely used for predicting the spatial-temporal occurrence of landslides. The reasons may be attributed to: 1) the bias characterizing near real-time satellite precipitation estimates, which is temporally varying not consistently year-by-year (being dependent on the satellite sensors used for obtaining the estimates), 2) the spatial/temporal resolution, 3) the timeliness, which is often insufficient for operational purposes, and 4) a general (often not justified) skepticism in the use of satellite products for land applications (Brocca et al., 2017; AghaKouchak et al., 2015). Satellite-based precipitation records have been made available since ~15 years, spanning a period of > 30 years and with a spatial-temporal resolution that might be appropriate for landslide studies. Arguably, due to the limited spatial representativeness of point information from rain gauges, the spatial issue of remote sensing products related to their coarse resolution is also encountered with ground-based observations. However, as mentioned above, currently rain gauges are the only source of information used in landslide early warning system. Here, we test the use of satellite-based rainfall estimates through a comparative analysis of satellite-based rainfall product with rain gauge measurements.

On this basis, we intend to address here the following scientific question: How far are we from the use of satellite rainfall products for landslide forecasting? Indeed, we believe that there is a lot of unexplored potential in using such data sets for landslide prediction. Their importance will be invaluable in developing countries where early warning systems for landslides are much more useful, and needed. Connected to the main scientific question, the following objectives are explored: which satellite-based rainfall product performs best in terms of landslide prediction? How to evaluate the quality of satellite-based rainfall products in the context of landslides?

To address the above questions, we perform a thorough study in Italy where detailed information about the occurrence of landslide events is available (Brunetti et al., 2015; Peruccacci et al., 2017). Specifically, we explore a catalogue listing 1414 rainfall-induced landslides in Italy, in the 7-year period 2008–2014. Four different satellite-based precipitation products are considered: 1) 3B42-RT (version 7) by the Tropical Rainfall Measurement Mission (TRMM) Multi-satellite Precipitation Analysis, TMPA (Huffman et al., 2007), 2) SM2RAIN-ASCAT product (http://dx.doi.org/10.13140/RG.2.2.10955.18728) that is based on the application of SM2RAIN algorithm (Brocca et al., 2014) to ASCAT (Advanced SCATterometer) SM product (Wagner et al., 2013), 3) Precipitation Estimation from Remotely Sensed Information using Artificial Neural Network (PERSIANN, Hsu et al., 1997), and 4) the Climate Prediction Center (CPC) Morphing Technique (CMORPH, Joyce et al., 2004). In addition, a ground-based rainfall data set obtained from a dense network of rain gauges (~3000) spanning the entire Italian territory is used as reference (Ciabatta et al., 2017). To assess the reliability of the different rainfall products (satellite- and ground-based), their relative performance in landslides detection is compared by using the well-established *ED* threshold approach (Peruccacci et al., 2017). We note that such a system is used for the rainfall-induced landslide forecast within the National Department of Civil Protection in Italy (Rossi et al., 2012). Therefore, the results of this study could have an impact also for operational landslide forecasting systems. However, our main purpose here is to assess the quality of satellite-based precipitation products in Italy where we have detailed information on landslides events and an established modeling system.

2. Study area

Italy is a boot-shaped peninsula that extends for about 300,000 km^2 in the Mediterranean Sea including the major islands of Sicily and

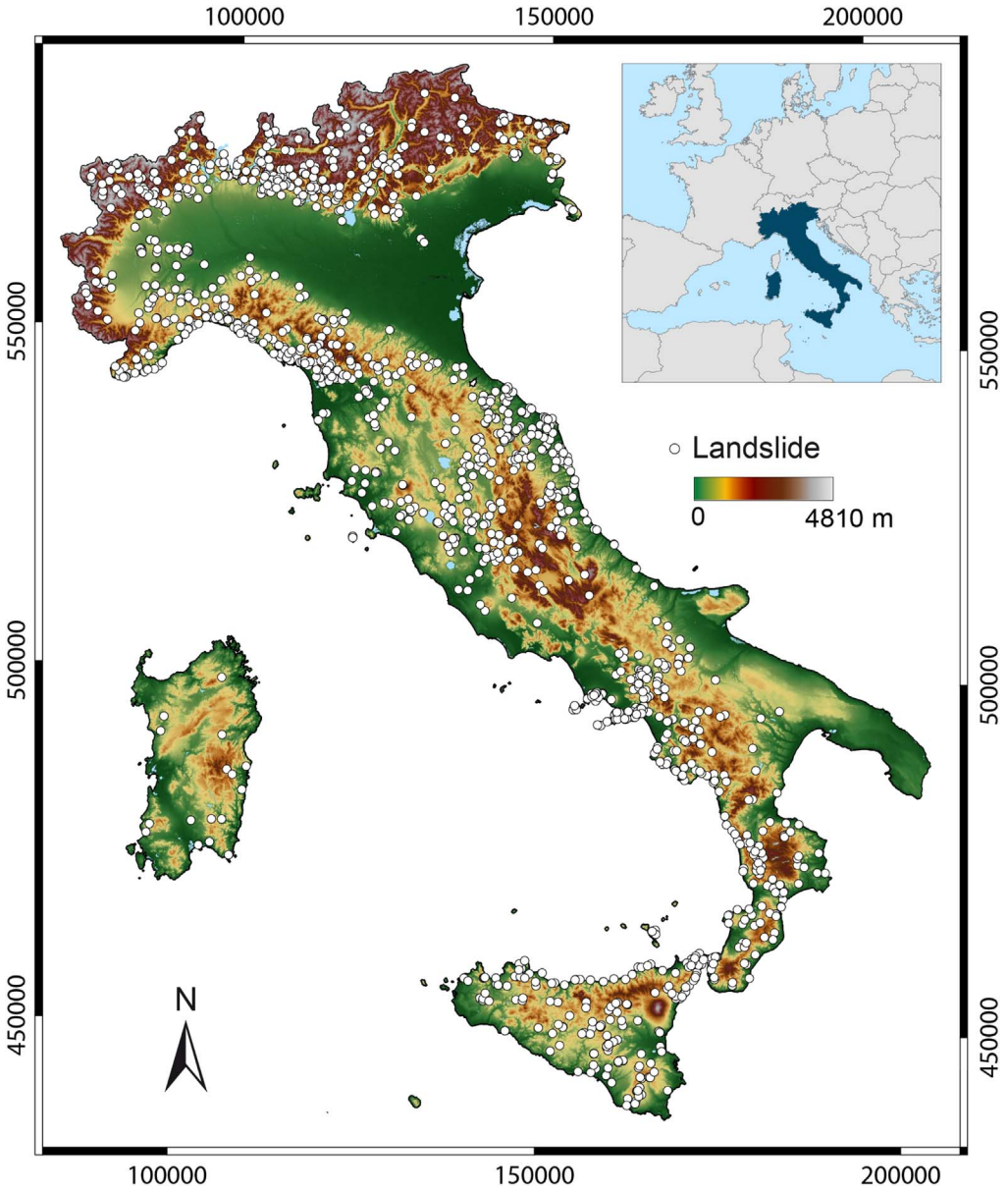

Fig. 1. Map of Italy showing the distribution of the rainfall-induced landslides in the period 2008–2014 (white dots).

Sardinia (Fig. 1).

Given its location and latitude, climate varies largely from northern to southern Italy. The coldest period occurs in December and January, the hottest in July and August. In the northern part of Italy, which includes the Po River Valley and the Alps mountain range, the climate is typically cold in winter and warm in summer with abundant rain. Snowfalls are common in autumn and spring over 1500 m on the Alps. Along the peninsula and in the islands the climate is temperate, with cold winters and dry summers with mean temperature increasing going southward. Mean annual precipitation ranges from < 400 mm in Sicily and Sardinia, to > 2000 mm in the northern Apennines and the eastern Alps. Generally, November is the wettest and July the driest month (Desiato et al., 2015).

Except for the Po River Valley and narrow coastal belts, the Italian mainland is generally hilly and mountainous. The topography causes widespread and frequent landslides, actually more than half a million recognized and mapped (Trigila et al., 2015). Most of the failures occur after intense or prolonged rainfall (Guzzetti et al., 1994; Guzzetti and Tonelli, 2004).

3. Data and methods

3.1. Landslide and rainfall data

Landslide information is obtained from a catalogue of rainfall events responsible for failures in Italy collected by Peruccacci et al. (2017). We use a subset of 1414 rainfall-induced landslides in the 7-year period between 2008 and 2014 that matches the time interval of rainfall information available from satellite estimates used in this study.

Landslide information is derived from digital and printed newspapers, blogs, technical documents, and landslide event reports. The documented rainfall-induced landslides are mapped as single points, using Google Earth™ (white dots in Fig. 1).

Each landslide in the catalogue has a temporal accuracy in three classes. The first class contains failures for which the exact time (hourly) of occurrence is known, while the second and the third classes include landslides for which the part of the day or the day of occurrence is inferred, respectively.

As mentioned above, we use here one rain gauge and four satellite-based rainfall data sets. The rain gauge based product, hereinafter OBS,

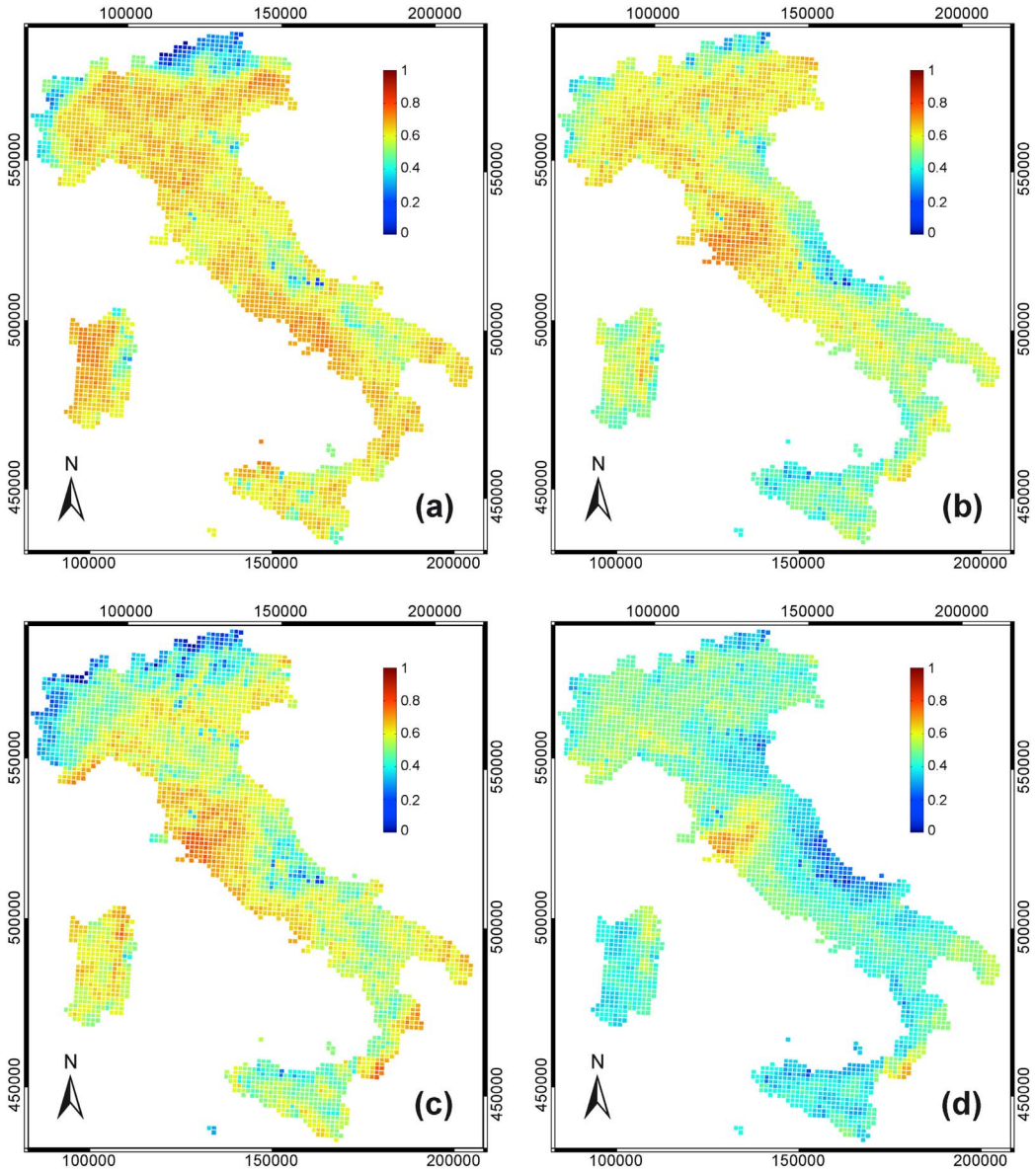

Fig. 2. Maps of Pearson's correlation between ground-based rainfall observations (OBS) and (a) SM2RASC, (b) 3B42-RT, (c) CMORPH and (d) PERSIANN satellite rainfall products.

is obtained from the Italian Civil Protection Department meteorological monitoring network. This data set is obtained by interpolating via an advanced kriging technique the data from about 3000 rain gauges available throughout the Italian territory (Pignone et al., 2010). The data set provides hourly rainfall observations over a grid with spacing of 10 km (Ciabatta et al., 2017). Although this source of information is impacted by spatial representation issues, here, we consider OBS data set as "reference".

The TMPA 3B42-RT product (Huffman et al., 2007, hereinafter 3B42-RT), version 7 (http://trmm.gsfc.nasa.gov), is obtained by combining rainfall estimates from various satellite sensors. The multi-satellite platform uses the TRMM Microwave Imager (TMI), the Special Sensor Microwave Imager (SSM/I) on board the Defense Meteorological Satellite Program (DMSP) satellites, the Advanced Microwave Scanning Radiometer EOS, AMSR-E, and the Advanced Microwave Sounding Unit-B (AMSU-B) on board the National Oceanic and Atmospheric Administration (NOAA) satellite series. In addition, the 3B42-RT product also uses Geostationary (GEO) Infrared data, characterized by higher spatial and temporal resolution than the microwave data, through a constellation of GEO satellites. The 3B42-RT product is provided by the National Aeronautics and Space Administration (NASA) with a temporal resolution of 3 h and a spatial resolution of 0.25° (~25 km) for the ± 50° north–south latitude band with a latency of about 8 h.

The SM2RASC product is obtained through the application of the SM2RAIN (Brocca et al., 2013, 2014) algorithm to the ASCAT SM data set. The SM data are obtained from the Metop-A and -B satellite, and they are characterized by a spatial resolution of 25 km, enhanced to 12.5 km after observation resampling, and a daily temporal resolution. The SM2RASC product has been specifically developed for Italy during the period 2008–2015 over the 12.5 km grid with daily temporal resolution. More in details, the algorithm has been applied to the H109 product provided by the H SAF project (http://hsaf.meteoam.it/) and has been calibrated during the period 2013–2014 against ground-based observations. Due to the temporal resolution of SM2RASC, the product shows limitations in the definitions of shorter precipitation events (at sub-daily). The algorithm is also not able to estimate rainfall where the soil is close to saturation, as in such conditions, no variation of the soil water content can be observed during a rainfall event. Finally, the quality of rainfall estimation is strictly related to the quality of SM input data. SM retrievals over complex topography or densely vegetated areas are characterized by low quality and should be used carefully. Nevertheless, the product showed good capabilities in identifying rainfall at

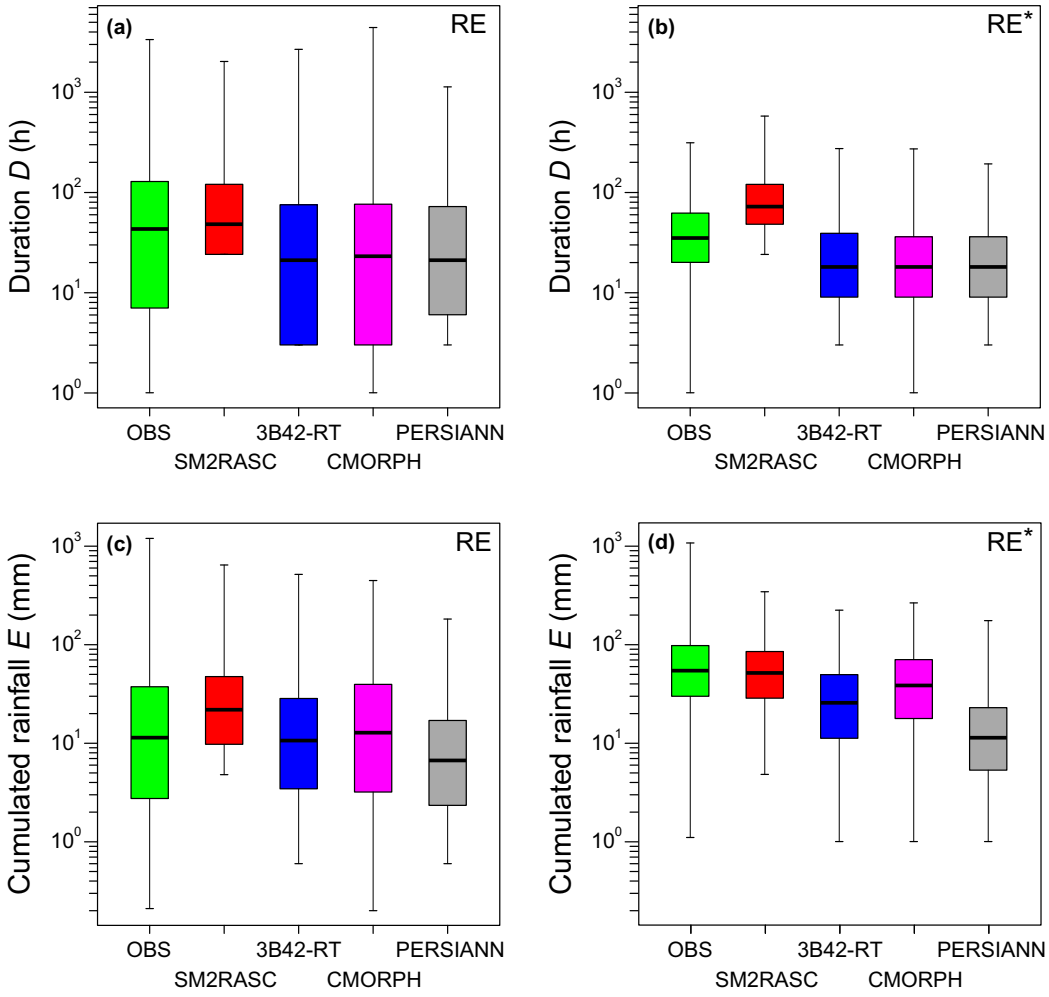

Fig. 3. Comparison between the box plot for (a) the rainfall duration D and (b) the cumulated rainfall E of RE and RE* for OBS (green), SM2RASC (red), 3B42-RT (blue), CMORPH (magenta) and PERSIANN (gray) data sets. (For interpretation of the references to color in this figure legend, the reader is referred to the web version of this article.)

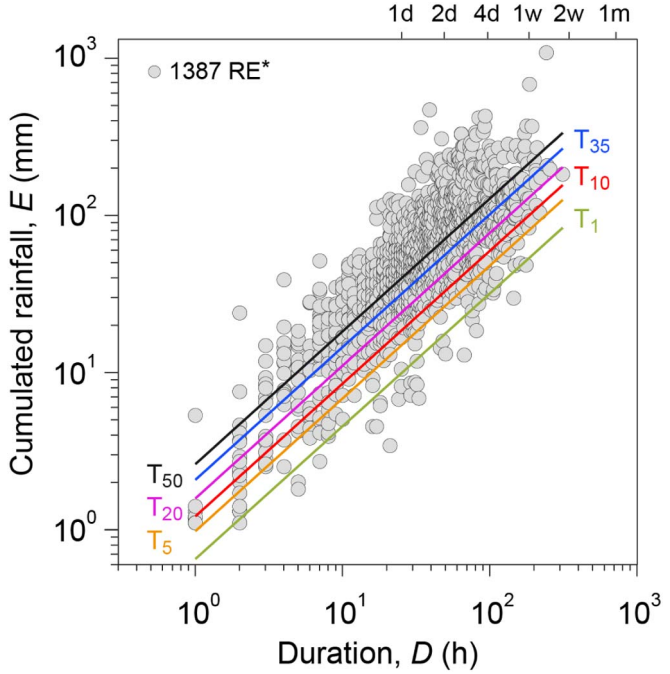

Fig. 4. Example of *ED* rainfall thresholds calculated using RE* at exceeding probabilities from 1% (T_1) to 50% (T_{50}) for the OBS data set. Light gray dots are the (D,E) pairs.

daily temporal resolution, as shown in Ciabatta et al. (2015, 2017).

CMORPH rainfall estimates are obtained by exploiting the same microwave sensors used for 3B42-RT rainfall product; the infrared data are used to fill the gap at the times between two successive microwave satellite overpasses, through morphing technique. The product is provided by the Climate Prediction Center (CPC) of the National Oceanic and Atmospheric Administration (NOAA) at the spatial resolutions of 0.25° and 8 km on a daily, 3-hourly or 30-minute basis for the ± 60° latitude band. Here we used the high resolution product (8 km at the equator every 30 min) obtained via interpolation of individual satellite-derived estimates (~12 × 15 km). For further details regarding CMORPH rainfall product, the readers are referred to Joyce et al. (2004). The product is provided about 18 h after observation.

PERSIANN (Hsu et al., 1997) data set uses the artificial neural network technique to estimate rainfall rate from geostationary infrared data at each 0.25° pixel at different temporal resolutions, for the ± 60° latitude band. In this work, the 3-hour temporal resolution is chosen. Rainfall estimation is carried out by training the infrared data to the collocated microwave estimates, when available. The product is developed by the Center for Hydrometeorology and Remote Sensing of University of California, Irvine, and it is available since March 2000 (http://chrsdata.eng.uci.edu/) about 2 days after observations.

The accuracy of 3B42-RT, PERSIANN and CMORPH depends mostly on the quality of the passive microwave and infrared precipitation retrievals, and particularly on the availability of frequent satellite overpasses over the region of interest (Nijssen and Lettenmaier, 2004). If the

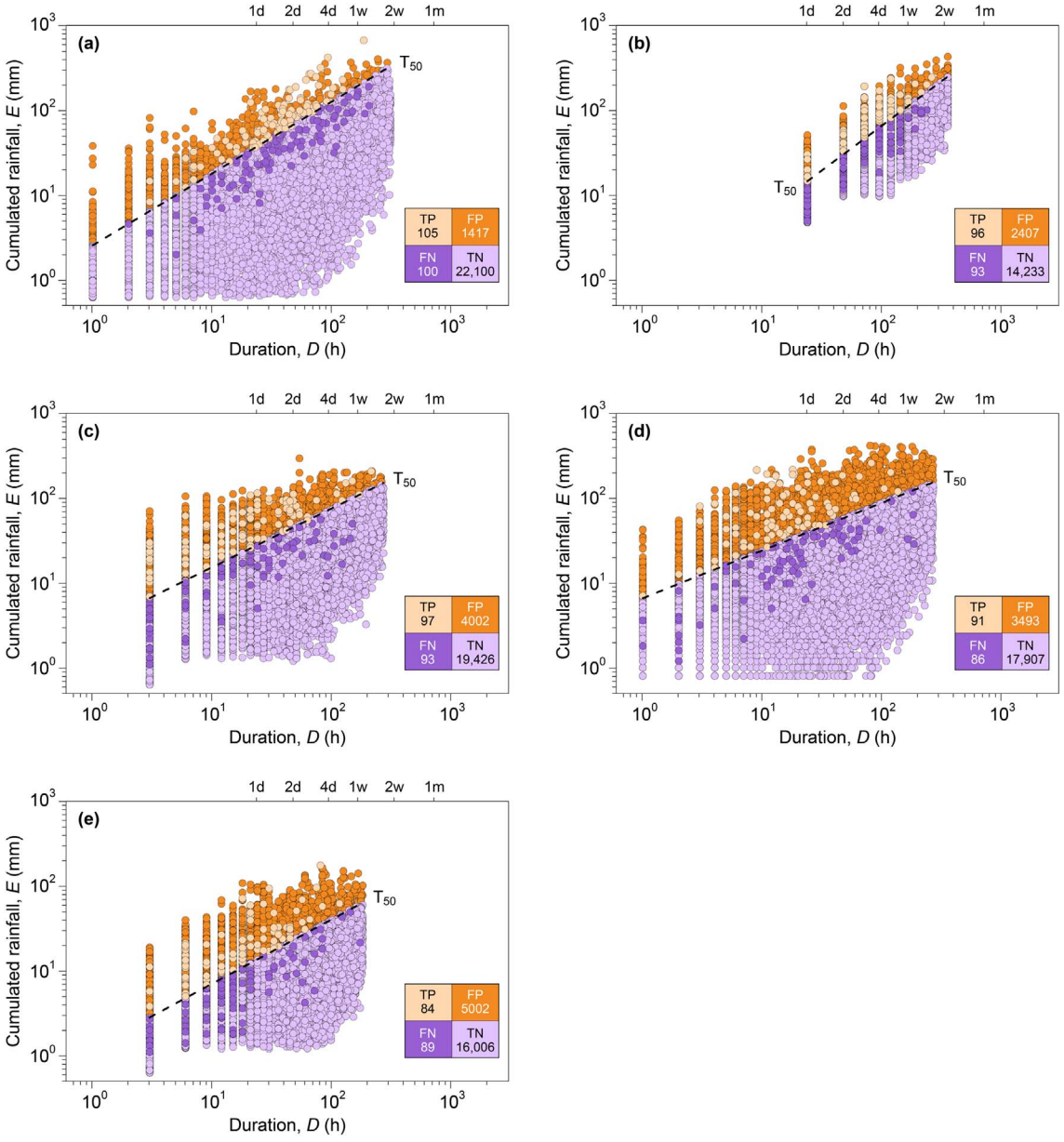

Fig. 5. Rainfall duration vs. cumulated event rainfall conditions in Italy in the period 2008–2014, compared with thresholds at 50% ($T_{50\%}$) non-exceedance probability level (dashed black lines) for (a) OBS, (b) SM2RASC, (c) 3B42-RT, (d) CMORPH and (e) PERSIANN. Legend: TP, true positives; TN, true negative; FP, false positive; FN, false negative.

overpasses frequency is not sufficiently high, a rainfall event could be underestimated or completely missed (Ciabatta et al., 2017).

For this study, we decided to consider the best spatial and temporal resolution of each satellite-based product (except CMORPH that is slightly degraded from ~8 km, 30 min to 10 km, 1 h). Therefore, we choose an analysis grid with spacing of 10 km to which all the products are interpolated through the nearest neighboring approach that does not change the spatial pattern of coarser resolution products (i.e., 3B42-RT, PERSIANN and SM2RASC). In terms of temporal resolution, we consider the native temporal sampling of each satellite rainfall products, i.e. the 3-hour blocks for 3B42-RT and PERSIANN and 24-h block for SM2RASC. The CMORPH product is aggregated at hourly resolution (originally at 30 min).

3.2. Algorithm for rainfall event reconstruction

The algorithm proposed by Melillo et al. (2015) is exploited to calculate the rainfall responsible for the observed landslides. For the purpose, the algorithm analyzes the daily rainfall obtained from ground-based stations and satellite sensors, and reconstructs distinct rainfall events (RE) in terms of their duration D (in h) and cumulated rainfall E (in mm), i.e. (D, E) pairs. In particular, to separate two consecutive rainfall events the algorithm requires a minimum dry period (i.e., a period without rainfall or with a negligible amount of rainfall). The length of the dry period varies depending on the local seasonal and climatic conditions. Specifically, dry periods of 48 h (two days) and 96 h (four days) are used to identify rainfall events in the warm and in the cold season, respectively (Peruccacci et al., 2017). After reconstructing RE, and with the information on the occurrence day of each landslide and on the rainfall of the pixel containing the landslide, the algorithm identifies the rainfall events responsible for each failure (RE*). Note, that when the landslide occurs after the end of the event the corresponding RE* is equivalent to RE. Otherwise, the duration of RE* is shorter than that of RE, and the cumulated rainfall is lower (Melillo et al., 2015). For each data set, we discard those RE* having a delay between the rainfall ending time and the landslide occurrence

(a)

OBS			
(%)	POD	POFD	HK
3	0.96	0.37	0.59
5	0.95	0.32	0.63
10	**0.90**	**0.25**	**0.65**
15	**0.84**	**0.20**	**0.65**
20	0.80	0.17	0.63
25	0.76	0.14	0.62
30	0.73	0.12	0.61
35	0.68	0.10	0.57
40	0.63	0.09	0.54
45	0.57	0.08	0.49
50	0.52	0.07	0.46

(b)

SM2RASC			
(%)	POD	POFD	HK
3	0.97	0.80	0.18
5	0.96	0.72	0.24
10	0.89	0.53	0.36
15	0.86	0.46	0.40
20	**0.82**	**0.39**	**0.43**
25	**0.76**	**0.33**	**0.43**
30	0.71	0.28	0.42
35	0.64	0.25	0.39
40	0.59	0.21	0.39
45	0.53	0.18	0.35
50	0.48	0.15	0.33

(c)

3B42-RT			
(%)	POD	POFD	HK
3	0.96	0.70	0.26
5	0.94	0.63	0.30
10	0.89	0.52	0.37
15	0.84	0.45	0.39
20	**0.80**	**0.39**	**0.41**
25	**0.76**	**0.34**	**0.41**
30	0.70	0.30	0.40
35	0.64	0.26	0.38
40	0.60	0.23	0.37
45	0.56	0.20	0.36
50	0.49	0.17	0.32

(d)

CMORPH			
(%)	POD	POFD	HK
3	0.97	0.66	0.31
5	0.94	0.60	0.35
10	0.90	0.49	0.40
15	0.85	0.42	0.42
20	**0.79**	**0.37**	**0.43**
25	**0.75**	**0.32**	**0.43**
30	0.70	0.28	0.42
35	0.65	0.25	0.41
40	0.61	0.22	0.39
45	0.57	0.19	0.38
50	0.51	0.16	0.35

(e)

PERSIANN			
(%)	POD	POFD	HK
3	0.98	0.85	0.13
5	0.97	0.77	0.20
10	0.90	0.65	0.26
15	0.84	0.56	0.28
20	0.78	0.49	0.29
25	**0.75**	**0.44**	**0.31**
30	0.69	0.39	0.30
35	0.65	0.34	0.30
40	0.59	0.31	0.28
45	0.55	0.27	0.28
50	0.49	0.24	0.25

Fig. 6. Values of the POD, POFD and HK skill scores obtained varying the threshold non-exceedance probability for the five data sets. Values in red are those that maximize HK. (For interpretation of the references to color in this figure legend, the reader is referred to the web version of this article.)

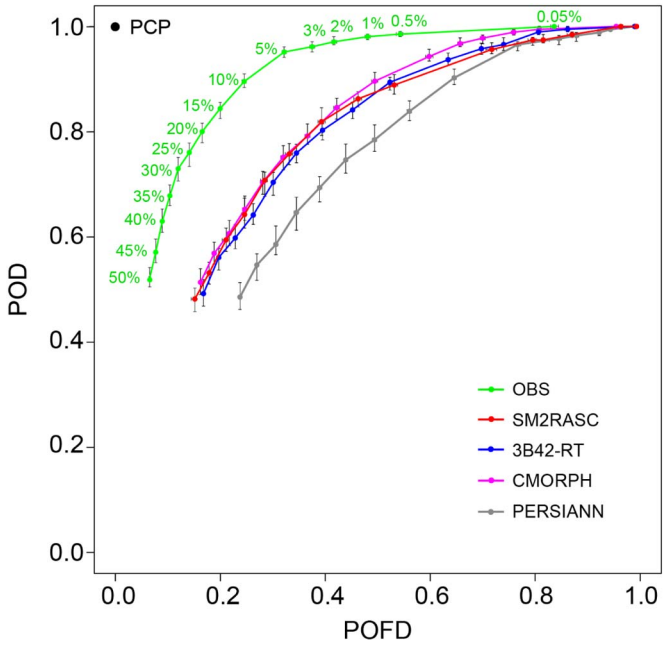

Fig. 7. ROC curves built by skill scores obtained varying the threshold non-exceedance probability for OBS (green), SM2RASC (red), 3B42-RT (blue), CMORPH (magenta) and PERSIANN (gray) data sets. Horizontal and vertical bars represent the range of variation of POFD and POD for the 100 runs in which RE* are randomly selected. (For interpretation of the references to color in this figure legend, the reader is referred to the web version of this article.)

Table 1
Rainfall *ED* thresholds for the possible initiation of landslides in Italy.

Data set	Threshold name	Threshold equation	Duration range (h)
OBS	$T_{20,OBS}$	$E = (1.6 \pm 0.1) \times D^{(0.84 \pm 0.02)}$	1–312
SM2RASC	$T_{20,SM2RASC}$	$E = (0.3 \pm 0.1) \times D^{(1.05 \pm 0.02)}$	24–360
3B42-RT	$T_{20,3B42\text{-}RT}$	$E = (1.6 \pm 0.1) \times D^{(0.69 \pm 0.02)}$	3–273
CMORPH	$T_{20,CMORPH}$	$E = (3.2 \pm 0.3) \times D^{(0.56 \pm 0.03)}$	1–271
PERSIANN	$T_{20,PERSIANN}$	$E = (0.7 \pm 0.1) \times D^{(0.76 \pm 0.03)}$	3–183

time longer than 48 h. This should prevent the use of wrong information (i.e., incorrectly dated landslides) in the definition of the thresholds.

The reconstructed RE* for OBS, SM2RASC, 3B42-RT, CMORPH and PERSIANN data sets are analyzed to define empirical rainfall thresholds for the possible initiation of landslides in Italy. Note that the number of RE* is less than the number of landslides since in some cases the rainfall measured before the failure was null.

3.3. Method for calculation and selection of ED rainfall thresholds

To calculate the empirical cumulated event rainfall-rainfall duration (*ED*) thresholds for the five data sets, we adopt the well-established frequentist method proposed by Brunetti et al. (2010), and modified by Peruccacci et al. (2012). The method assumes in a Cartesian plane the threshold curve of the form:

$$E = (\alpha \pm \Delta\alpha) \cdot D^{(\gamma \pm \Delta\gamma)} \quad (1)$$

where E is the cumulated rainfall (in mm), D the rainfall duration (in hours), α is a scaling constant (the intercept), γ is the shape parameter (that defines the slope of the power law curve), and $\Delta\alpha$ and $\Delta\gamma$ represent the uncertainties of α and γ, respectively. The method determines thresholds for any non-exceedance probability level, e.g., a threshold at 5% probability level leaves 5% of the (D,E) pairs with landslides below the curve.

In order to determine the non-exceedance probability providing the best performance in landslide forecasting we use the following validation procedure. For each rainfall data set (OBS, SM2RASC, 3B42-RT, CMORPH, and PERSIANN), we construct synthetic series randomly selecting 85% of rainfall events with landslides (RE*). Then, we use the remaining 15% of RE* to assess the threshold performance. For the purpose, rainfall thresholds are used as binary classifiers of rainfall events that triggered (RE*) or did not trigger landslides. In a *DE* plane, a RE* located above the threshold is a true positive (TP), and below the threshold is a false negative (FN). Analogously, a rainfall event without landslides above the threshold is a false positive (FP), and below is a true negative (TN). We repeat 100 times the random selection of rainfall events, and we get a contingency table with the mean values of TP, FN, FP and TN.

As the threshold non-exceedance probability rises, the number of FN increases, and the number of TP decreases correspondingly. Conversely, when lowering the threshold non-exceedance probability, the number of FP increases and the number of TN decreases. In case the thresholds are used in a landslide warning system, FP results in “false alarms” and FN in “missed alarms”. It is worth noting that FP can be overrated by the lack of information on landslide occurrence i.e., landslides may have occurred but not reported. Consequently, even the number of TN can be overestimated (Gariano et al., 2015). In addition, we would notice that the validation of the rainfall thresholds is a complicated issue; at first glance, the occurrence of a rainfall-induced landslide is a stochastic mechanism, i.e. the same rainfall conditions may trigger a landslide in an area and may not in a different place. Indeed, the prediction of rainfall-induced landslide does not depend exclusively upon correct rainfall forecasts (and measurements), it is instead largely influenced by the local characteristics of the terrain (slope, soil type, soil moisture, etc.), which are mostly unknown for large areas.

From the contingency table, we obtain, the POD (Probability Of Detection) and the POFD (Probability Of False Detection) skill scores:

$$POD = \frac{TP}{TP + FN} \quad (2)$$

$$POFD = \frac{FP}{FP + TN} \quad (3)$$

More specifically, POD (or Hit Rate) is the fraction of RE* above the threshold, i.e. predicted correctly, and POFD (or False Alarm Rate) is the fraction of RE above the threshold, i.e. predicted incorrectly. We use POD and POFD to draw the receiver operating characteristic (ROC) curves (Fawcett, 2006) and to calculate the HK (i.e., the difference POD-POFD) skill score (Hanssen and Kuiper, 1965). The quality of the satellite-based rainfall product is evaluated by comparing the ROC curves and the HK skill score whose optimal value is 1.

4. Results

In the following, we assess the capability of the satellite-based rainfall products to forecast rainfall-induced landslides using the ground-based rainfall product as a reference. Based on the statistical criteria described above, we compare the performances of SM2RASC, 3B42-RT, CMORPH and PERSIANN data sets. In addition, we evaluate the best performing threshold for each product calculating skill scores and ROC.

As a preliminary analysis, we investigate the performance of the four satellite rainfall products against ground observations for the whole period of analysis. Specifically, we compute the temporal Pearson's correlation between OBS and satellite-based rainfall for each pixel and results are shown in Fig. 2. The correlation maps clearly show that the SM2RASC product (Fig. 2a) has generally improved performances with respect to the other products. For instance, the median correlation for the whole Italian territory is equal to 0.60 for SM2RASC, 0.55 for 3B42-RT and CMORPH and 0.42 for PERSIANN. All the

products perform poorly over the Alps and high mountainous areas in central Italy; 3B42-RT (Fig. 2b) and CMORPH (Fig. 2c) perform very similarly with better correlations in central Italy while SM2RASC is the best product over southern Italy (Fig. 2a).

Fig. 3 shows the box plots of the duration D (Fig. 3a and b) and of the cumulated rainfall E (Fig. 3c and d) for RE and RE* calculated using the ground-based and satellite-based data sets.

Inspection of Fig. 3a reveals that OBS and SM2RASC rainfall events (RE) exhibit a similar median value of D, whereas 3B42-RT, CMORPH and PERSIANN rainfall events have a shorter duration. The duration of RE* for SM2RASC is longer than that in other data sets (Fig. 3b) likely due to its temporal resolution (24 h). From Fig. 3c it is evident that the E median value for 3B42-RT and CMORPH is comparable to that of OBS. Not surprisingly, the E median value for SM2RASC is higher since the rainfall is cumulated every 24 h. Fig. 3d shows that satellite products generally underestimate the cumulated rainfall responsible for the failures measured by OBS, except for SM2RASC. As expected, for all the products E for RE* (Fig. 3d) is generally higher than E for RE (Fig. 3c).

Applying the frequentist method to the synthetic series obtained using 85% of the reconstructed RE* (Section 3.3), we calculate the mean ED rainfall thresholds at different non-exceedance probabilities for the four data sets. An example of thresholds for the OBS data set is shown in Fig. 4.

Using the remaining 15% of RE*, we simulate the application of the thresholds in a hypothetical landslide warning system. Fig. 5 portrays, as an example, the classification of rainfall events in the four contingencies (TP, FP, FN and TN) based on the 50% rainfall thresholds for the five data sets. Each graph in Fig. 5 represents one out of 100 synthetic series.

Applying the classification illustrated in Fig. 5 to the different non-exceedance probability levels, we find POD and POFD skill scores. For civil protection purposes, the priority is to minimize the number of missed alarms (FN) and secondary to limit false alarms (FP), which means maximizing POD and minimizing POFD, i.e. maximizing HK. Fig. 6 shows for each data set the POD, POFD and HK values at different non-exceedance probability.

Following this criterion for each data set, we select the threshold probability level that maximizes the HK skill score. For OBS the highest HK is obtained with the threshold at 10% non-exceedance probability that also maximizes the POD value; for the satellite-based data sets except PERSIANN, the highest HK with the maximum POD is obtained with the threshold at 20%. The threshold at 25% is the most suitable for PERSIANN. Using POD and POFD, we also build the ROC. Fig. 7 shows the comparison between the ROC curves for the five data sets. As expected, OBS gives the best performance at all the non-exceedance probability levels. Among the curves of satellite-based rainfall data, CMORPH and SM2RASC are performing slightly better than 3B42-RT, while PERSIANN is the worst.

In order to compare the thresholds of ground-based and satellite-based data, Table 1 shows the equations at 20% non-exceedance probability. The OBS data set exhibits the highest threshold, except for $D < \sim 12$ h, where the CMORPH curve is slightly higher. We acknowledge here that the comparison could be unfair when dealing with different data sources and resolution.

5. Discussion and conclusions

In this study, we compared different satellite rainfall products to address the following question: how far are we from the use of satellite rainfall products in landslide forecasting? For the purpose, we developed a specific procedure that simulates the use of satellite (and observed) rainfall data in a hypothetical landslide warning system. Based on this procedure, we are able to infer the potential of the satellite rainfall products in predicting landslides occurrence.

Results shown in Fig. 3 underline that satellite rainfall products, except SM2RASC, tend to underestimate observed rainfall, especially in terms of rainfall events responsible for the landslides (Fig. 3d). This result is somehow expected as the OBS data set is obtained by the interpolation of point rainfall measurements (from rain gauges) and, hence, larger rainfall intensities are expected with respect to the satellite rainfall products that provide a spatially averaged measurement at the pixel scale. We maintain that such underestimation is not an issue in the development of a landslide warning system based on satellite data. Indeed, the underestimation will result in a lower threshold curve in the DE plane (Rossi et al., 2017), as shown in Table 1, but the product performance in terms of capability of detecting rainfall events resulting in landslide failure is not affected. Certainly, the underestimation is not a problem if it is spatially and temporally homogeneous. Differently, if satellite rainfall products are biased in particular regimes (e.g., orographic rainfall) or in particular locations (e.g., dense vegetated areas for SM2RASC), the accuracy of the warning system is significantly affected.

In order to assess the satellite rainfall products for landslide forecasting, results shown in Figs. 5–7 should be evaluated. We constructed standard contingency tables that are used to determine if the considered rainfall product is able to correctly identify landslide events. Therefore, we computed the specific categorical scores (POD and POFD) and then we performed a ROC analysis. By analyzing results in Figs. 6 and 7, interesting conclusion can be drawn. Indeed, we obtained, as expected, that the OBS rainfall data set (from ground observations) provides the best results. Then CMORPH and SM2RASC are found to be the best performing satellite rainfall products, followed by 3B42-RT that provides similar results, and finally PERSIANN is performing the worst.

Based on these results, we can conclude that the temporal resolution is an important factor for forecasting landslides. Indeed, the occurrence time of the landslide is highly relevant, and the use of daily aggregated data may produce a significant overestimation of the rainfall needed to trigger the landslide if it is occurring at the beginning of the day. On the one hand, PERSIANN is performing worst according to its low correlations with long-term rainfall observations as shown in Fig. 2. On the other hand, SM2RASC is the best product in reproducing rainfall observations (Fig. 2), even though this may be partly attributed to its calibration over the study area. The same product is not the best one in terms of landslide forecasting due to its daily temporal resolution. To assess this aspect, we performed also computations by aggregating all satellite rainfall products at daily time resolution (not shown for brevity) and in this case, SM2RASC is found to be the best satellite rainfall product also in terms of landslide forecasting. Therefore, the higher temporal resolution of CMORPH and 3B42-RT, and their good accuracy, is likely the main reason for the obtained results. In future studies, the integration of CMORPH (or 3B42-RT) and SM2RASC will be also investigated (see e.g., Ciabatta et al., 2015, 2017; Chiaravalloti et al., 2018), as we expect that the complementarity of the two satellite rainfall products will bring to improved performances.

In terms of spatial resolution, we expected that the 8-km resolution CMORPH product would have obtained the best results. However, as the propagation in time of rainfall estimates is carried out by using infrared measurements, less accurate than microwave sensors for rainfall retrieval, it is possible that the enhanced temporal resolution brings to lower accuracy. This might be an explanation for the unexpected result, but further studies are needed to fully understand this behavior.

In summary, in order to reply to the original scientific question, we believe that satellite rainfall products considered here are able to satisfactorily predict landslide occurrence in Italy (see Fig. 6), and the lower performance with respect to ground observations are due to the high-quality of OBS data set (based on ~3000 rain gauges). In Italy, the satellite-based rainfall estimates will never replace the ground-based measurements, which provide the most accurate landslide prediction. Indeed, we anticipate that the obtained results will have a more important use in scarcely gauged regions (e.g., developing countries), and

a global scale dedicated study will be the natural next step of this research activity. This task will face several issues, like the availability of ground rainfall data and landslide catalogue. While the first point could be addressed by considering global precipitation data sets (e.g., Beck et al., 2017) and by taking the non-homogenous spatial distribution of rainfall stations into account, the latter point will use global landslide catalogue, as the one described by Kirschbaum (2014). We expect that satellite rainfall estimates might be an important additional data source for developing continental or global landslide warning systems.

Acknowledgements

Massimo Melillo was supported by a grant of the Italian National Department for Civil Protection (Accordi di Collaborazione 2015, 2016). We are grateful to Simone Gabellani and Mauro Rossi for providing the gridded rainfall data set over the Italian territory. We thank the support of the Italian Department for Civil Protection in this activity. We are grateful to the three anonymous reviewers for their helpful comments on improving the early version of the manuscript.

References

AghaKouchak, A., Farahmand, A., Melton, F.S., Teixeira, J., Anderson, M.C., Wardlow, B.D., Hain, C.R., 2015. Remote sensing of drought: progress, challenges and opportunities. Rev. Geophys. 53 (2), 452–480. http://dx.doi.org/10.1002/2014RG000456.

Aleotti, P., 2004. A warning system for rainfall-induced shallow failures. Eng. Geol. 73, 247–265. http://dx.doi.org/10.1016/j.enggeo.2004.01.007.

Alvioli, M., Baum, R.L., 2016. Parallelization of the TRIGRS model for rainfall-induced landslides using the message passing interface. Environ. Model. Softw. 81, 122–135. http://dx.doi.org/10.1016/j.envsoft.2016.04.002.

Baum, R.L., Godt, J.W., 2010. Early warning of rainfall-induced shallow landslides and debris flows in the USA. Landslides 7, 259–272. http://dx.doi.org/10.1007/s10346-009-0177-0.

Baum, R.L., Godt, J.W., Savage, W.Z., 2010. Estimating the timing and location of shallow rainfall-induced landslides using a model for transient, unsaturated infiltration. J. Geophys. Res. 115, F03013. http://dx.doi.org/10.1029/2009JF001321.

Beck, H.E., Vergopolan, N., Pan, M., Levizzani, V., van Dijk, A.I.J.M., Weedon, G., Brocca, L., Pappenberger, F., Huffman, G.J., Wood, E.F., 2017. Global-scale evaluation of 22 precipitation datasets using gauge observations and hydrological modeling. Hydrol. Earth Syst. Sci. 21, 6201–6217. http://dx.doi.org/10.5194/hess-21-6201-2017.

Berti, M., Martina, M.L.V., Franceschini, S., Pignone, S., Simoni, A., Pizziolo, M., 2012. Probabilistic rainfall thresholds for landslide occurrence using a Bayesian approach. J. Geophys. Res. 117, F04006. http://dx.doi.org/10.1029/2012JF002367.

Brocca, L., Ponziani, F., Moramarco, T., Melone, F., Berni, N., Wagner, W., 2012. Improving landslide forecasting using ASCAT-derived soil moisture data: a case study of the Torgiovannetto landslide in central Italy. Remote Sens. 4 (5), 1232–1244. http://dx.doi.org/10.3390/rs4051232.

Brocca, L., Melone, F., Moramarco, T., Wagner, W., 2013. A new method for rainfall estimation through soil moisture observations. Geophys. Res. Lett. 40 (5), 853–858. http://dx.doi.org/10.1002/grl.50173.

Brocca, L., Ciabatta, L., Massari, C., Moramarco, T., Hahn, S., Hasenauer, S., Kidd, R., Dorigo, W., Wagner, W., Levizzani, V., 2014. Soil as a natural rain gauge: estimating global rainfall from satellite soil moisture data. J. Geophys. Res. 119 (9), 5128–5141. http://dx.doi.org/10.1002/2014JD021489.

Brocca, L., Crow, W.T., Ciabatta, L., Massari, C., de Rosnay, P., Enenkel, M., Hahn, S., Amarnath, G., Camici, S., Tarpanelli, A., Wagner, W., 2017. A review of the applications of ASCAT soil moisture products. IEEE J. Sel. Top. Appl. Earth Obs. Remote Sens. 10 (5), 2285–2306. http://dx.doi.org/10.1109/JSTARS.2017.2651140.

Brunetti, M.T., Perruccacci, S., Rossi, M., Luciani, S., Valigi, D., Guzzetti, F., 2010. Rainfall thresholds for the possible occurrence of landslides in Italy. Nat. Hazards Earth Syst. Sci. 10, 447–458. http://dx.doi.org/10.5194/nhess-10-447-2010.

Brunetti, M.T., Peruccacci, S., Antronico, L., Bartolini, D., Deganutti, A.M., Gariano, S.L., Iovine, G., Luciani, S., Luino, F., Melillo, M., Palladino, M.R., Parise, M., Rossi, M., Turconi, L., Vennari, C., Vessia, G., Viero, A., Guzzetti, F., 2015. Catalogue of rainfall events with shallow landslides and new rainfall thresholds in Italy. In: Lollino, G., Giordan, D., Crosta, G.B., Corominas, J., Azzam, R., Wasowski, J., Sciarra, N. (Eds.), Springer Special Series: Engineering Geology 340 for Society and Territory. Landslide Processes Volume 2. pp. 1575–1579. http://dx.doi.org/10.1007/978-3-319-09057-3_280.

Caine, N., 1980. The rainfall intensity-duration control of shallow landslides and debris flows. Geogr. Ann. 62, 23–27. http://dx.doi.org/10.2307/520449.

Chen, C.W., Saito, H., Oguchi, T., 2017. Analyzing rainfall-induced mass movements in Taiwan using the soil water index. Landslides 14 (3), 1031–1041. http://dx.doi.org/10.1007/s10346-016-0788-1.

Chiaravalloti, F., Brocca, L., Procopio, A., Massari, C., Gabriele, S., 2018. Assessment of GPM and SM2RAIN-ASCAT rainfall products over complex terrain in southern Italy. Atmos. Res. 206, 64–74. http://dx.doi.org/10.1016/j.atmosres.2018.02.019.

Ciabatta, L., Brocca, L., Massari, C., Moramarco, T., Puca, S., Rinollo, A., Gabellani, S., Wagner, W., 2015. Integration of satellite soil moisture and rainfall observations over the Italian territory. J. Hydrometeorol. 16, 1341–1355. http://dx.doi.org/10.1175/JHM-D-14-0108.1.

Ciabatta, L., Camici, S., Brocca, L., Ponziani, F., Stelluti, M., Berni, N., Moramarco, T., 2016. Assessing the impact of climate-change scenarios on landslide occurrence in Umbria region, Italy. J. Hydrol. 541, 285–295. http://dx.doi.org/10.1016/j.jhydrol.2016.02.007.

Ciabatta, L., Marra, A.C., Panegrossi, G., Casella, D., Sanò, P., Dietrich, S., Massari, C., Brocca, L., 2017. Daily precipitation estimation through different microwave sensors: verification study over Italy. J. Hydrol. 545, 436–450. http://dx.doi.org/10.1016/j.jhydrol.2016.12.057.

Crozier, M.J., 1999. Prediction of rainfall-triggered landslides: a test of the antecedent water status model. Earth Surf. Process. Landf. 24, 825–833. http://dx.doi.org/10.1002/(SICI)1096-9837(199908)24:9<825::AID-ESP14>3.3.CO;2-D.

Cullen, A.C., Al-Suhili, R., Khanbilvardi, R., 2016. Guidance index for shallow landslide hazard analysis. Remote Sens. 8 (10), 866. http://dx.doi.org/10.3390/rs8100866.

Desiato, F., Fioravanti, G., Fraschetti, P., Perconti, W., Piervitali, E., 2015. Valori climatici normali di temperatura e precipitazione in Italia. ISPRA, Stato dell'Ambiente 55/2014. (ISBN 978-88-448-0689-7 (in Italian)).

Farahmand, A., AghaKouchak, A., 2013. A satellite-based global landslide model. Nat. Hazards Earth Syst. Sci. 13, 1259–1267. http://dx.doi.org/10.5194/nhess-13-1259-2013.

Fawcett, T., 2006. An introduction to ROC analysis. Pattern Recogn. Lett. 27, 861–874. http://dx.doi.org/10.1016/j.patrec.2005.10.010.

Fischer, E.M., Knutti, R., 2015. Anthropogenic contribution to global occurrence of heavy-precipitation and high-temperature extremes. Nat. Clim. Chang. 5, 560–564. http://dx.doi.org/10.1038/nclimate2617.

Gariano, S.L., Guzzetti, F., 2016. Landslides in a changing climate. Earth Sci. Rev. 162, 227–252. http://dx.doi.org/10.1016/j.earscirev.2016.08.011.

Gariano, S.L., Brunetti, M.T., Iovine, G., Melillo, M., Peruccacci, S., Terranova, O., Vennari, C., Guzzetti, F., 2015. Calibration and validation of rainfall thresholds for shallow landslide forecasting in Sicily, southern Italy. Geomorphology 228, 653–665. http://dx.doi.org/10.1016/j.geomorph.2014.10.019.

Giannecchini, R., Galanti, Y., D'Amato Avanzi, G., Barsanti, M., 2016. Probabilistic rainfall thresholds for triggering debris flows in a human-modified landscape. Geomorphology 257, 94–107. http://dx.doi.org/10.1016/j.geomorph.2015.12.012.

Glade, T., Crozier, M.J., Smith, P., 2000. Applying probability determination to refine landslide-triggering rainfall thresholds using an empirical "antecedent daily rainfall model". Pure Appl. Geophys. 157 (6/8), 1059–1079. http://dx.doi.org/10.1007/s000240050017.

Guzzetti, F., Tonelli, G., 2004. Information system on hydrological and geomorphological catastrophes in Italy (SICI): a tool for managing landslide and flood hazards. Nat. Hazards Earth Syst. Sci. 4, 213–232. http://dx.doi.org/10.5194/nhess-4-213-2004.

Guzzetti, F., Cardinali, M., Reichenbach, P., 1994. The AVI project: a bibliographical and archive inventory of landslides and floods in Italy. Environ. Manag. 18, 623–633. http://dx.doi.org/10.1007/bf02400865.

Guzzetti, F., Stark, C.P., Salvati, P., 2005. Evaluation of flood and landslide risk to the population of Italy. Environ. Manag. 36 (1), 15–36. http://dx.doi.org/10.1007/s00267-003-0257-1.

Guzzetti, F., Peruccacci, S., Rossi, M., Stark, C.P., 2007. Rainfall thresholds for the initiation of landslides in central and southern Europe. Meteorol. Atmos. Phys. 98, 239–267. http://dx.doi.org/10.1007/s00703-007-0262-7.

Guzzetti, F., Peruccacci, S., Rossi, M., Stark, C.P., 2008. The rainfall intensity-duration control of shallow landslides and debris flow: an update. Landslides 5, 3–17. http://dx.doi.org/10.1007/s10346-007-0112-1.

Hanssen, A.W., Kuipers, W.J.A., 1965. On the relationship between the frequency of rain and various meteorological parameters, Koninklijk Nederlands Meteorologisch Institut, Meded. Verhand. 81. pp. 86.

Hong, Y., Adler, R., Huffman, G., 2006. Evaluation of the potential of NASA multi-satellite precipitation analysis in global landslide hazard assessment. Geophys. Res. Lett. 33, L22402. http://dx.doi.org/10.1029/2006GL028010.

Hong, Y., Adler, R., Huffman, G., 2007. Use of satellite remote sensing data in the mapping of global landslide susceptibility. Nat. Hazards 43, 245–256. http://dx.doi.org/10.1007/s11069-006-9104-z.

Hou, A.Y., Kakar, R.K., Neeck, S., Azarbarzin, A.A., Kummerow, C.D., Kojima, M., Oki, R., Nakamura, K., Iguchi, T., 2014. The Global Precipitation Measurement (GPM) mission. Bull. Am. Meteorol. Soc. 95 (5), 701–722. http://dx.doi.org/10.1175/BAMS-D-13-00164.1.

Hsu, K., Gao, X., Sorooshian, S., Gupta, H.V., 1997. Precipitation estimation from remotely sensed information using artificial neural networks. J. Appl. Meteorol. 36 (9), 1176–1190.

Huffman, G.J., Adler, R.F., Bolvin, D.T., Gu, G., Nelkin, E.J., Bowman, K.P., Hong, Y., Stocker, E.F., Wolff, D.B., 2007. The TRMM multisatellite precipitation analysis (TMPA): quasi global, multiyear, combined-sensor precipitation estimates at fine scales. J. Hydrometeorol. 8 (1), 38–55. http://dx.doi.org/10.1175/JHM560.1.

Innes, J.L., 1983. Debris flows. Prog. Phys. Geogr. 7, 469–501. http://dx.doi.org/10.1177/030913338300700401.

Joyce, R.J., Janowiak, J.E., Arkin, P.A., Xie, P., 2004. CMORPH: a method that produces global precipitation estimates from passive microwave and infrared data at high spatial and temporal resolution. J. Hydrometeorol. 5, 487–503.

Keefer, D.K., Wilson, R.C., Mark, R.K., Brabb, E.E., Brown, W.M.-I.I.I., Ellen, S.D., Harp, E.L., Wieczorek, G.F., Alger, C.S., Zatkin, R.S., 1987. Real-time landslide warning during heavy rainfall. Science 238, 921–925. http://dx.doi.org/10.1126/science.238.4829.921.

Kidd, C., Becker, A., Huffman, G., Muller, C., Joe, P., Skofronick-Jackson, G., Kirschbaum, D., 2017. So, how much of the Earth's surface is covered by rain gauges? Bull. Am. Meteorol. Soc. 98, 69–78. http://dx.doi.org/10.1175/BAMS-D-14-00283.1.

Kirschbaum, D.B., 2014. Global catalog of rainfall-triggered landslides for spatial and temporal hazard characterization. In: Sassa, K., Canuti, P., Yin, Y. (Eds.), Landslide Science for a Safer Geoenvironment. Springer, Cham (ISBN 978-3-319-05050-8). https://doi.org/10.1007/978-3-319-05050-8_125.

Kirschbaum, D.B., Adler, R., Hong, Y., Lerner-Lam, A., 2009. Evaluation of a preliminary satellite-based landslide hazard algorithm using global landslide inventories. Nat. Hazards Earth Syst. Sci. 9 (3), 673–686. http://dx.doi.org/10.5194/nhess-9-673-2009.

Kirschbaum, D.B., Adler, R., Hong, Y., Kumar, S., Peters-Lidard, C., Lerner-Lam, A., 2012. Advances in landslide nowcasting: evaluation of a global and regional modeling approach. Environ. Earth Sci. 66 (6), 1683–1696. http://dx.doi.org/10.1007/s12665-011-0990-3.

Kirschbaum, D.B., Stanley, T., Simmons, J., 2015. A dynamic landslide hazard assessment system for central America and Hispaniola. Nat. Hazards Earth Syst. Sci. 15 (10), 2257–2272. http://dx.doi.org/10.5194/nhess-15-2257-2015.

Lagomarsino, D., Segoni, S., Fanti, R., Catani, F., 2013. Updating and tuning a regional scale landslide early warning system. Landslides 10, 91–97. http://dx.doi.org/10.1007/s10346-012-0376-y.

Lepore, C., Arnone, E., Noto, L.V., Sivandran, G., Bras, R.L., 2013. Physically based modeling of rainfall triggered landslides: a case study in the Luquillo forest, Puerto Rico. Hydrol. Earth Syst. Sci. 17 (9), 3371–3387. http://dx.doi.org/10.5194/hess-17-3371-2013.

Liao, Z., Hong, Y., Wang, J., Fukuoka, H., Sassa, K., Karnawati, D., Fathani, F., 2010. Prototyping an experimental early warning system for rainfall-induced landslides in Indonesia using satellite remote sensing and geospatial datasets. Landslides 7 (3), 317–324. http://dx.doi.org/10.1007/s10346-010-0219-7.

Marra, F., Destro, E., Nikolopoulos, E.I., Zoccatelli, D., Creutin, J.D., Guzzetti, F., Borga, M., 2017a. Impact of rainfall spatial aggregation on the identification of debris flow occurrence thresholds. Hydrol. Earth Syst. Sci. 21, 4525–4532. http://dx.doi.org/10.5194/hess-21-4525-2017.

Marra, F., Morin, E., Peleg, N., Mei, Y., Anagnostou, E.N., 2017b. Intensity–duration–frequency curves from remote sensing rainfall estimates: comparing satellite and weather radar over the eastern Mediterranean. Hydrol. Earth Syst. Sci. 21, 2389–2404. http://dx.doi.org/10.5194/hess-21-2389-2017.

Martelloni, G., Segoni, S., Fanti, R., Catani, F., 2012. Rainfall thresholds for the forecasting of landslide occurrence at regional scale. Landslides 9, 485–495. http://dx.doi.org/10.1007/s10346-011-0308-2.

Melillo, M., Brunetti, M.T., Peruccacci, S., Gariano, S.L., Guzzetti, F., 2015. An algorithm for the objective reconstruction of rainfall events responsible for landslides. Landslides 12, 311–320. http://dx.doi.org/10.1007/s10346-014-0471-3.

Mugnai, A., et al., 2013. Precipitation products from the hydrology SAF. Nat. Hazards Earth Syst. Sci. 13, 1959–1981. http://dx.doi.org/10.5194/nhess-13-1959-2013.

Nijssen, B., Lettenmaier, D.P., 2004. Effect of precipitation sampling error on simulated hydrological fluxes and states: anticipating the global precipitation measurement satellites. J. Geophys. Res.-Atmos. 109, D02103. http://dx.doi.org/10.1029/2003JD003497.

Nikolopoulos, E.I., Crema, S., Marchi, L., Marra, F., Guzzetti, F., Borga, M., 2014. Impact of uncertainty in rainfall estimation on the identification of rainfall thresholds for debris flow occurrence. Geomorphology 221, 286–297. https://doi.org/10.1016/j.geomorph.2014.06.015.

Nikolopoulos, E.I., Destro, E., Maggioni, V., Marra, F., Borga, M., 2017. Satellite rainfall estimates for debris flow prediction: an evaluation based on rainfall accumulation–duration thresholds. J. Hydrometeorol. 18 (8), 2207–2214. https://doi.org/10.1175/JHM-D-17-0052.1.

Peruccacci, S., Brunetti, M.T., Luciani, S., Vennari, C., Guzzetti, F., 2012. Lithological and seasonal control on rainfall thresholds for the possible initiation of landslides in central Italy. Geomorphology 139, 79–90. http://dx.doi.org/10.1016/j.geomorph.2011.10.005.

Peruccacci, S., Brunetti, M.T., Gariano, S.L., Melillo, M., Rossi, M., Guzzetti, F., 2017. Rainfall thresholds for possible landslide occurrence in Italy. Geomorphology 290, 39–57. http://dx.doi.org/10.1016/j.geomorph.2017.03.031.

Piciullo, L., Gariano, S.L., Melillo, M., Brunetti, M.T., Peruccacci, S., Guzzetti, F., Calvello, M., 2016. Definition and performance of a threshold-based regional early warning model for rainfall-induced landslides. Landslides. http://dx.doi.org/10.1007/s10346-016-0750-2.

Pignone, F., Rebora, N., Silvestro, F., Castelli, F., 2010. GRISO–Rain. Operational Agreement 778/2009 DPC-CIMA, Year-1 Activity Rep. 272/2010. CIMA Research Foundation, Savona, Italy (353 pp.).

Ponziani, F., Pandolfo, C., Stelluti, M., Berni, N., Brocca, L., Moramarco, T., 2011. Assessment of rainfall thresholds and soil moisture modeling for operational hydrogeological risk prevention in the Umbria region (central Italy). Landslides 9 (2), 229–237. http://dx.doi.org/10.1007/s10346-011-0287-3.

Posner, A.J., Georgakakos, K.P., 2015. Soil moisture and precipitation thresholds for real-time landslide prediction in El Salvador. Landslides 12, 1179. http://dx.doi.org/10.1007/s10346-015-0618-x.

Ray, R.L., Jacobs, J.M., 2007. Relationships among remotely sensed soil moisture, precipitation and landslide events. Nat. Hazards 43 (2), 211–222. http://dx.doi.org/10.1007/s11069-006-9095-9.

Robbins, J.C., 2016. A probabilistic approach for assessing landslide-triggering event rainfall in Papua New Guinea, using TRMM satellite precipitation estimates. J. Hydrol. 541, 296–309. http://dx.doi.org/10.1016/j.jhydrol.2016.06.052.

Rosi, A., Segoni, S., Catani, F., Casagli, N., 2012. Statistical and environmental analyses for the definition of a regional rainfall threshold system for landslide triggering in Tuscany (Italy). J. Geogr. Sci. 22 (4), 617–629. http://dx.doi.org/10.1007/s11442-012-0951-0.

Rossi, M., Peruccacci, S., Brunetti, M.T., Marchesini, I., Luciani, S., Ardizzone, F., Balducci, V., Bianchi, C., Cardinali, M., Fiorucci, F., Mondini, A.C., Reichenbach, P., Salvati, P., Santangelo, M., Bartolini, D., Gariano, S.L., Palladino, M., Vessia, G., Viero, A., Antronico, L., Borselli, L., Deganutti, A.M., Iovine, G., Luino, F., Parise, M., Polemio, M., Guzzetti, F., 2012. SANF: national warning system for rainfall-induced landslides in Italy. In: Eberhardt, E., Froese, C., Turner, A.K., Leroueil, S. (Eds.), Landslides and Engineered Slopes: Protecting Society Through Improved Understanding. Taylor & Francis Group, London, pp. 1895–1899 (ISBN: 978-0-415-62123-6).

Rossi, M., Luciani, S., Valigi, D., Kirschbaum, D., Brunetti, M.T., Peruccacci, S., Guzzetti, F., 2017. Statistical approaches for the definition of landslide rainfall thresholds and their uncertainty using rain gauge and satellite data. Geomorphology 285, 16–27. http://dx.doi.org/10.1016/j.geomorph.2017.02.001.

Salvati, P., Bianchi, C., Fiorucci, F., Giostrella, P., Marchesini, I., Guzzetti, F., 2014. Perception of flood and landslide risk in Italy: a preliminary analysis. Nat. Hazards Earth Syst. Sci. 14, 2589–2603. http://dx.doi.org/10.5194/nhess-14-2589-2014.

Segoni, S., Leoni, L., Benedetti, A.I., Catani, F., Righini, G., et al., 2010. Towards a definition of a real-time forecasting network for rainfall induced shallow landslides. Nat. Hazards Earth Syst. Sci. 9, 2119–2133. http://dx.doi.org/10.5194/nhess-9-2119-2009.

Segoni, S., Lagomarsino, D., Fanti, R., Moretti, S., Casagli, N., 2015. Integration of rainfall thresholds and susceptibility maps in the Emilia Romagna (Italy) regional-scale landslide warning system. Landslides 12, 773–785. http://dx.doi.org/10.1007/s10346-014-0502-0.

Sidder, A., 2016. Tracking landslide hazards around the world, pixel by pixel. Eos 97. http://dx.doi.org/10.1029/2016EO060583.

Sorooshian, S., Hsu, K., Gao, X., Gupta, H., Imam, B., Braithwaite, D., 2000. Evaluation of the PERSIANN system satellite-based estimates of tropical rainfall. Bull. Am. Meteorol. Soc. 81, 2035–2046. http://dx.doi.org/10.1175/1520-0477(2000)081<2035:EOPSSE>2.3.CO;2.

Trigila, A., Iadanza, C., Bussettini, M., Lastoria, B., Barbano, A., 2015. Dissesto idrogeologico in Italia: pericolosità e indicatori di rischio. Rapporto 2015, Istituto Superiore per la Protezione e la Ricerca Ambientale – ISPRA, Rapporti 233/2015. (162 pp. (in Italian)).

Vennari, C., Gariano, S.L., Antronico, L., Brunetti, M.T., Iovine, G., Peruccacci, S., Terranova, O., Guzzetti, F., 2014. Rainfall thresholds for shallow landslide occurrence in Calabria, southern Italy. Nat. Hazards Earth Syst. Sci. 14, 317–330. http://dx.doi.org/10.5194/nhess-14-317-2014.

Wagner, W., Hahn, S., Kidd, R., Melzer, T., Bartalis, Z., Hasenauer, S., Figa, J., de Rosnay, P., Jann, A., Schneider, S., Komma, J., Kubu, G., Brugger, K., Aubrecht, C., Zuger, J., Gangkofner, U., Kienberger, S., Brocca, L., Wang, Y., Bloeschl, G., Eitzinger, J., Steinnocher, K., Zeil, P., Rubel, F., 2013. The ASCAT soil moisture product: a review of its specifications, validation results, and emerging applications. Meteorol. Z. 22 (1), 5–33. http://dx.doi.org/10.1127/0941-2948/2013/0399.